

High harmonics generation by plasmonic field enhancement

Seung-Woo Kim^{*1}, Seungchul Kim¹, In-Yong Park¹, Jonghan Jin^{1,2}

¹ Ultrafast Optics for Ultraprecision Group, KAIST, Science Town, Daejeon 305-701. South Korea.

² Currently with Korea Research Institute of Standards and Science, Daejeon 305-340. South Korea.

* swk@kaist.ac.kr

ABSTRACT

High harmonic generation is a well-established optical method to produce coherent short-wavelength light in the ultraviolet and soft-X ray range. This nonlinear conversion process requires ultrashort pulse lasers of strong intensity exceeding the threshold of 10^{13} Wcm⁻² to ionize noble gas atoms. Chirped pulse amplification (CPA) is popularly used to increase the intensity power of a femtosecond laser produced from an oscillator. However, CPA requires long cavities for multi-staged power amplification, restricting its practical uses due to hardware bulkiness and fragility. Recently, we successfully exploited the phenomenon of localized surface plasmon resonance for high harmonic generation, which enables replacing CPA with a compact metallic nanostructure. Surface plasmon resonance induced in a well-designed nanostructure allows for intensity enhancement of the incident laser field more than 20 dB. For experimental validation, a 2D array of gold bowtie nanostructure was fabricated on a sapphire substrate by the focused-ion-beam process. By injection of argon and xenon gas atoms onto the bowtie nanostructure, high harmonics up to 21st order were produced while the incident laser intensity remains at only 10^{11} Wcm⁻². In conclusion, the approach of exploiting surface plasmons resonance offers an important advantage of hardware compactness in high harmonic generation.

Keywords: localized surface plasmon, local field enhancement, high harmonic generation, extreme ultra-violet, optical frequency comb,

1. INTRODUCTION

Coherent short wavelength light in the range of extreme ultraviolet or soft x-ray has high potential to lead future applications to advanced microscopy or lithography. High harmonic generation firstly observed in 1988 is a promising way of generating coherent short radiation with a small hardware setup configured on a laboratory optical table [1-3]. Generated high harmonics strongly depend on the driving laser field in their temporal and spatial coherence properties. To induce the high harmonic generation, more than the laser intensity of 10^{13} Wcm⁻² is required because this process is based on the atom ionization process. This laser intensity can't be acquired by single laser oscillator. By chirped pulse amplification (CPA), highly intense laser pulse could be attainable to activate the ionization dynamics of the atom [4-5]. But CPA based laser amplification causes optical complexity and reduction of pulse repetition rate. Recently, intracavity pulse amplification was suggested for maintaining original comb structure of femtosecond pulse laser with several tens of MHz repetition rate. But, it is not easy to extract high harmonic beams from the cavity, also requires a long external cavity [6-7].

This paper discusses the development of novel and simple method for high-harmonic generation that requires no extra cavities or laser pumping to amplify the femtosecond laser. This is achieved by exploiting the localized surface plasmon (LSP) induced by resonant plasmons within metallic bowtie nanostructures [8]. LSP can form electric field enhancement by collective oscillation of free electrons [9, 10]. In this investigation, we use bowtie shaped plasmonic nano antenna which consists of two triangular patches pacing its tip to tip. When the array of bowtie nanostructures is illuminated by ultra short pulse, the resonant motion of free electrons in nanostructure induced highly localized electric field enhancement at the gap of each bowtie nanostructure. Theoretically, the field enhancement factor of bowtie nano antenna exceeds 20 dB, which is sufficient intensity to produce high harmonics with a single laser oscillator.

The field enhancement value and volume of LSP strongly depend on geometrical parameters and material properties of nanostructure [11-13]. To investigate the relation between the geometrical parameters and LSP, we analyzed near-field distribution of bowtie nanostructure by modifying several geometrical parameters. Additionally, we

will discuss the effect of non-ideally sharp bowtie nanostructure caused by fabrication capabilities. FDTD (Finite-Difference Time-Domain) method was adopted for calculating Maxwell's equation to analyze near-field distribution. We fabricated designed nanostructures using Au thin film on a thin sapphire substrate with a focused ion beam. This nanostructure was used for enhancement of low power femtosecond pulse laser which has only 10^{11} Wcm⁻². In our experiments, the output beam emitted from a titanium-sapphire femtosecond oscillator (10-fs pulse duration) is directly focused on the nanostructures with an injection of noble gas. From the results, we obtained high harmonic spectrum up to 17th harmonics (47 nm in wavelength) with argon gas and 21st harmonics (38 nm in wavelength) with xenon gas.

2. DESIGN OF PLASMONIC NANODEVICE

Among plasmonic nanodevices for enhancing electric field, the optical nano antenna has high localized field enhancement at the gap of antenna. The rod antenna and bowtie antenna were widely used, because of their favorable properties that include high localized field enhancement and subwavelength field confinement [14, 15]. However, bowtie design offers more free electrons than rod antenna, so bowtie nano antenna has wider enhanced field distribution. As illustrated in Fig. 1, four design parameters, height (h), thickness (t), angle (θ) and gap (d) were characterized to analyze the near-field intensity distribution of bowtie nanostructure. These parameters were chosen to monitor near-field variation at the gap of bowtie. As excitation source was defined as pulse duration of 10 fs corresponding to full width half maximum spectral bandwidth of 94 nm which is centered at wavelength of 800 nm. The pulse was illuminated to normal to the triangular surface of bowtie with a linear polarization which is parallel to the height parameters. The material of bowtie was chosen as gold (Au) which is widely used for localized surface plasmon resonance with near-IR laser. The complex dielectric constant of gold was determined by modified Debye model [16]. The computational domain was divided by 1 nm cubic cell in all 3-dimensional area for a precise calculation. The calculating time step was set automatically as 1.9 attosecond. The surrounded material was set as vacuum and perfectly matched layer (PML) was used for absorbing undesired electromagnetic field at each boundary. For numerical convenience, two representative points were selected at the middle layer of thickness direction. One is the center point of the bowtie gap and the other is apex of the one triangular patch denoted in fig. 1.

By changing four geometrical parameters, we verified that localized field enhancement highly depends on geometrical parameters. Firstly, we examine the intensity enhancement factor by varying the height from 100 nm to 215 nm with 20 nm step. Maximum intensity enhancement factor was appeared at the height of 175 nm. In this calculation, other parameters were fixed as gap of 20 nm, thickness of 50 nm and angle of 30°.

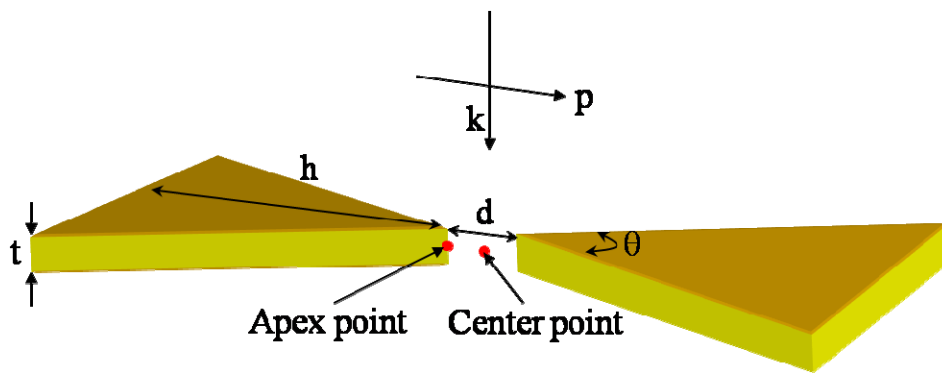


Fig. 1. FDTD simulation for plasmonic enhancement of a bowtie nanostructure characterized by four geometrical design parameters (height: h , thickness: t , apex angle: θ , separation gap: d). The incident direction (wave vector : k) and polarization (p) of the input femtosecond pulse laser are positioned as depicted in the figure in reference to the bowtie. Two representative points (Apex point, Center point) at the middle thickness layer are selected for comparison of the intensity enhancement factor around the separation gap of the bowtie nanostructure.

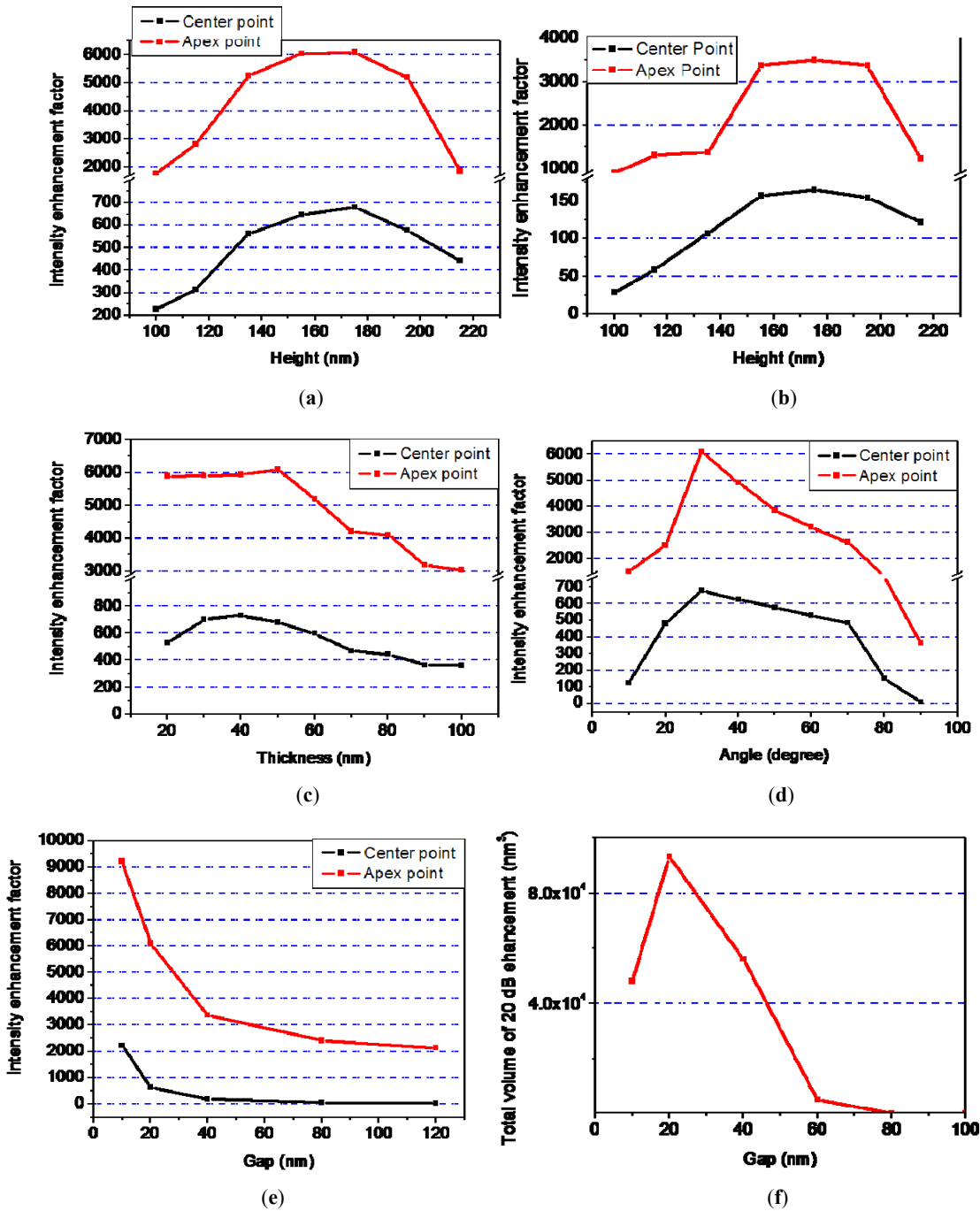


Fig. 2. Simulation results of the intensity enhancement factor computed at two representative locations: Center point and Apex point. In (a)~(e), red line indicates Apex point while black line is for Center point. (a) Height (h) is varied for a separation gap (d) of 20 nm, (b) Height (h) is varied for a separation gap (d) of 40 nm. (c) Variation of apex angle (d) Variation of thickness (e) Variation of separation gap. Other parameters except the varying parameter in each simulation were set constantly as height (h) of 175nm, apex angle of 30°, thickness of 50 nm, and separation gap of 20 nm. (f) Variation of the 20 dB volume with separation gap.

To verify the dependency between geometrical variables, we verified geometrical coupling between parameters. For example, when we change the gap value to 40 nm, overall magnitudes of intensity enhancement factor were decreased due to the weak interaction between tips. However, maximum intensity enhancement appeared at same height of 175 nm. Intuitively, the motion of free electrons along the height can be treated as vibration model with damping so resonant condition occurs at one specific height value [17]. This phenomenon also can be observed by the dependency of excited laser wavelength. When center wavelength of 1060 nm was excited to the bowtie nanostructure, maximum intensity enhancement factor appeared at height of 220 nm which is longer than shorter wavelength excitation. This means that the time for the free electron's movements along the height direction is related to the frequency of excited electromagnetic wave. The angle and thickness affect the amount of oscillating charges and spatial confinement of charges at the gap. In this simulation, height of 175 nm, angle of 30 ° and gap of 20 nm were set constantly. From the simulation results, bowtie nanostructure thicker than 40 nm makes less confinement of surface plasmons so intensity enhancement is decreased as increasing thickness of bowtie nanostructure. The narrow angle or wider angle is also related to the volume of accumulated surface plasmons. The variation of angle from 10 ° to 90 ° shows that angle of 30 ° makes most efficient enhancement at given conditions.

The effect for gap of bowtie was conducted by changing gap from 10 nm to 120 nm. For the smaller gap make higher intensity enhancement near the tip of each triangular patch, but enhanced near-field distribution is rapidly decreased for the bowtie with too narrow gap value. For the purpose of high harmonic generation, larger enhanced volume which has intensity over 10^{13} Wcm^{-2} is as important as higher enhancement factor. The volume of enhanced near-field is deeply related to the efficiency of high harmonic process. Therefore, final bowtie design was focused on maximize the volume of the intensity enhancement factor of 20 dB. For generation of high harmonics with a laser intensity of 10^{11} Wcm^{-2} , intensity enhancement factor of 20 dB is required in minimum. As shown in fig. 2(f), the gap narrower than 20 nm has small volume of intensity enhancement over 20 dB. As increasing the gap, the volume of intensity enhancement factor over 20 dB doesn't appear. From results, we chose the gap of the bowtie as 20 nm. Maximum intensity enhancement factor at gap of 10 nm has higher intensity enhancement factor than the case of gap of 20 nm, but nearly 2 times larger volume of intensity enhancement factor over 20 dB was achieved at the gap of 20 nm. Therefore, more high harmonic generation process could be triggered by the design with gap of 20 nm.

By considering previous simulations, we selected design parameters as height of 175 nm, thickness of 50 nm, angle of 30 ° and gap of 20 nm. The area of intensity enhancement factor over 20 dB was $60 \text{ nm} \times 50 \text{ nm} \times 50 \text{ nm}$ ($x \times y \times z$) in the gap between vertices. Fig. 3 shows calculated near-field distribution at the gap of bowtie. The enhanced near-field is decay as far from the tip of bowtie nanostructure. When we observe the temporal behavior of enhanced near-field at the gap, the shape of pulse is slightly different with the original input pulse. As plotted in fig. 4, the absolute phase, Φ_{ceo} which is the phase offset between carrier and envelope peak was initially set as 0. However, enhanced pulse at the gap shows different phase relation. Peak of carrier wave was shifted 90 ° in phase, therefore uniform absolute phase shift of 90 ° was appeared in results. Also, ring down effect was observed at the tail of pulse due to the high order dispersion.

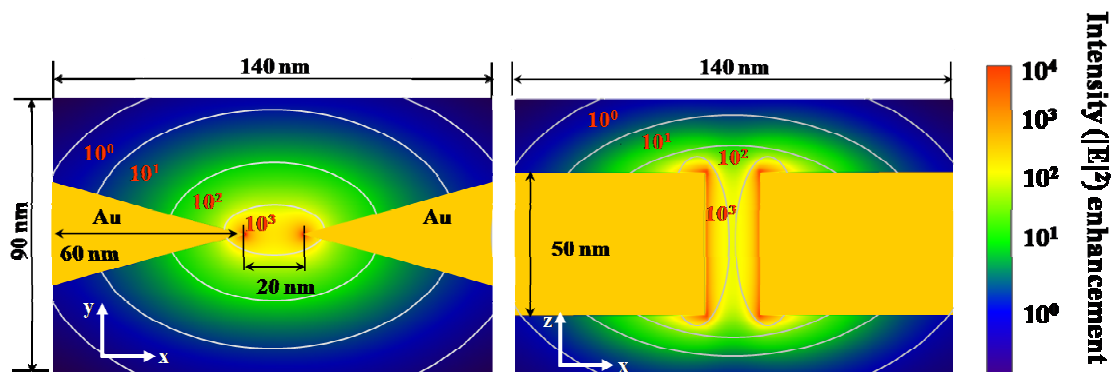


Fig. 3. Near field intensity distribution of the suggested bowtie nanostructure (height of 175 nm, gap of 20 nm, angle of 30 ° and thickness of 50 nm). The calculated near-field distribution shows a highly enhanced electromagnetic field more than 20 dB within a volume of $60 \text{ nm} \times 50 \text{ nm} \times 50 \text{ nm}$ ($x \times y \times z$) near the separation gap.

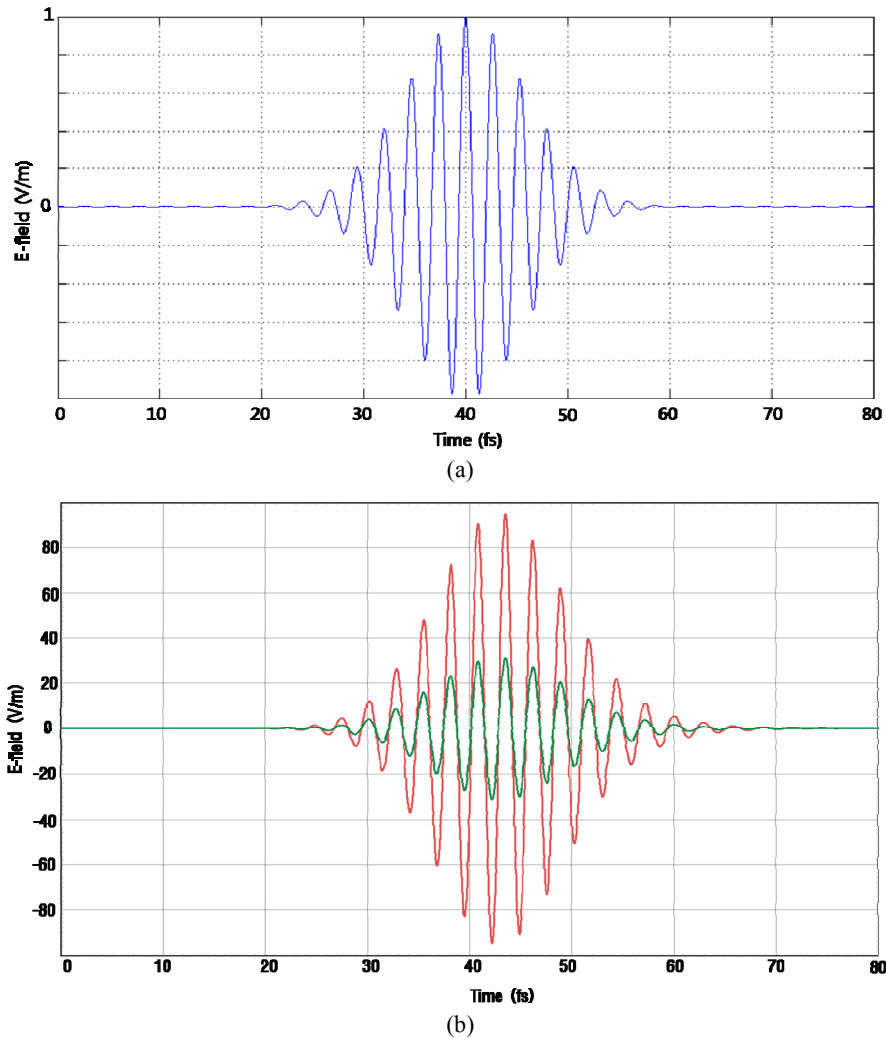


Fig. 4. (a) Temporal profile of the input pulse. (b) Temporal profiles of the induced plasmonic field enhancement at Center point(green pulse) and Apex point (red pulse). The induced enhancement fields have a uniform phase delay of 90° due to perfect resonance. Ring-down oscillation is observed at the tale of the induced fields in (b).

During the bowtie design, the apex of triangular patch were assumed as ideally sharp tip with 1 nm of cubic cell, but actual fabrication processes can not support such a sharp tip of bowtie nanostructure. Currently, focused ion beam milling process or E-beam lithography are widely known as a nanofabrication tool which has capability of sub 10 nm with highly stable conditions. Therefore, fabricated triangular patches have blunt edges. This can affect the degradation of plasmonic field enhancement at the gap of bowtie. For considering the effect on the blunt edge, calculations of two type of bowtie were performed. One is the rounded apex which diameter is changed from 5 nm to 50 nm by taking into consideration of fabrication results. The other type is flat apex that shape of each patch looks like a trapezium patch. Other geometrical dimensions were not changed for removing coupling between parameters, that is, bowtie has height of 175 nm, thickness of 50 nm, angle of 30° and gap of 20 nm. Fig. 5 shows tendency of intensity enhancement factors and the volume of 20 dB enhancement of two kinds of bowtie nanostructure. In fig. 5(a), the intensity enhancement factor at center point shows slow decrease, while the intensity enhancement factor at apex point exponentially decrease. These calculation results means that the electric field at apex point is made by dense electric flux which is highly depended on confinement of oscillating surface plasmons at each apex of triangular patch. However, electric field at center point is much affected by the interaction between two apexes, so slightly spreading surface plasmons in rounded apex can affect similar to surface plasmons of sharp tip. Interestingly, when the diameter of

rounded apex was increased as 50 nm, the volume of 20 dB intensity enhancement was the level of 60 % against ideal shape of bowtie. This means that high harmonic process can be occurred enough even though the diameter of rounded tip was increased to 50 nm. The volume of intensity enhancement is much related to the interaction between charges of both tips. Therefore, the height and the gap are more important parameters than the shape of apex. Also, same tendency of intensity enhancement factor by the flat apex was shown in fig. 5(c), (d). However, the decaying rate of intensity enhancement is slightly faster than the case of rounded apex.

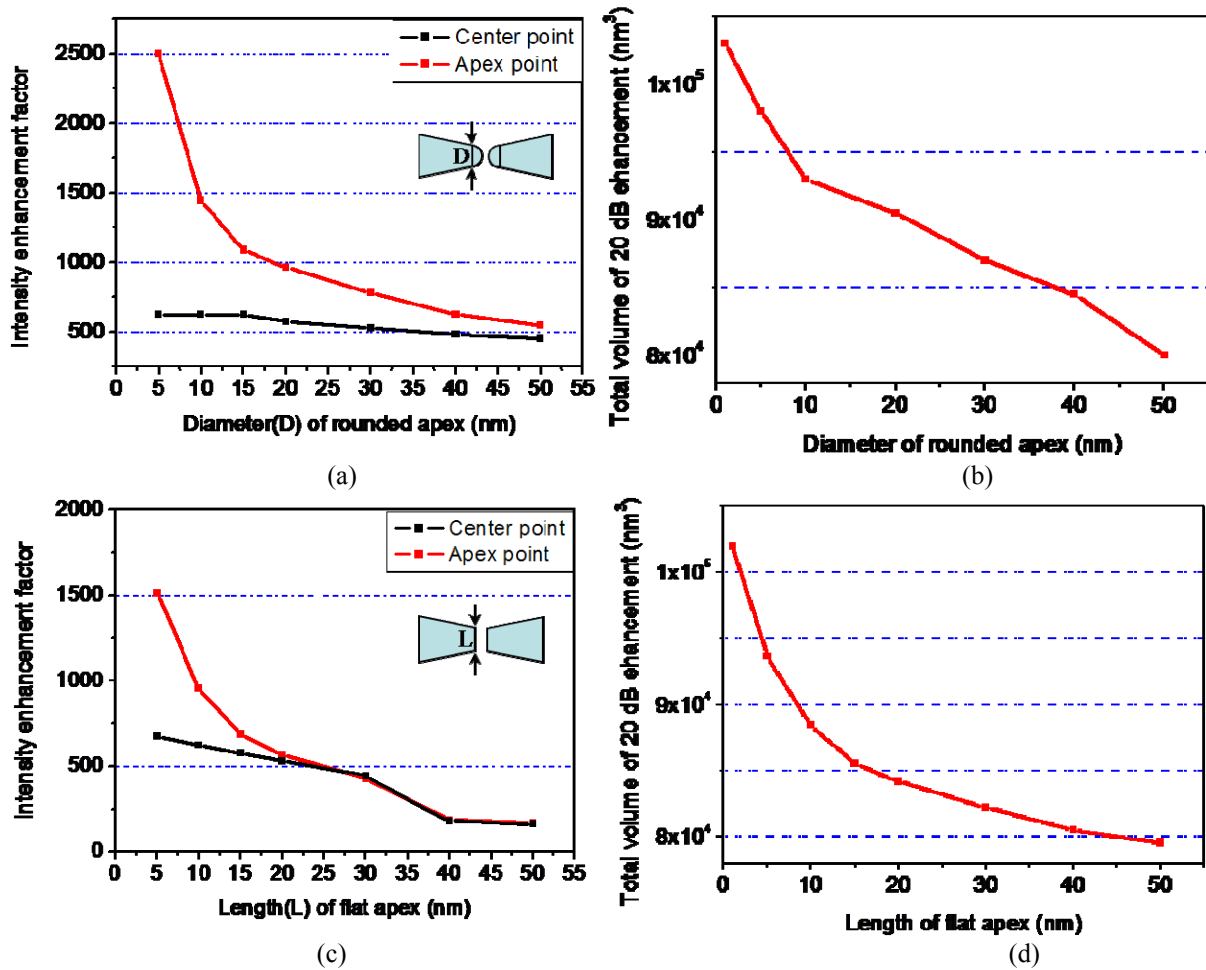


Fig. 5 FDTD calculation results for non-ideal tip shapes of bowtie nanostructure. D and L represent the diameters of the rounded apex (D) and the length of flat apex (L), respectively. Fig. 5(b), (d) are the calculated volumes of the intensity enhancement factor over 20 dB for the given shapes of bowtie nanostructure; (b) rounded bowtie and (d) trapezium bowtie.

3. FABRICATION OF PLASMONIC NANODEVICE

Fig. 6 is magnified image of fabricated 2D array of bowtie nanostructure using scanning electron microscope. As a specimen for bowtie fabrication, a 50 nm gold layer and a 5 nm chromium adhesion layer were evaporated on a 400 μm thick sapphire wafer. Sapphire substrate mainly used for holding each bowtie nanostructure and dissipating thermal

energies from bowties. Because sapphire has higher thermal conductivity than fused silica or quartz, it can reduce accumulated heat efficiently from bowtie nanostructures. The designated array of nanostructure was fabricated with focused ion beam (FIB) milling process. Beam conditions of focused ion beam (SMI 3050 TB) are acceleration voltage of 30 kV, current of 1 pA and the dwell time of 50 μ s. The current of FIB is related to the gaussian beam size of FIB, so lower current can make fine structure.

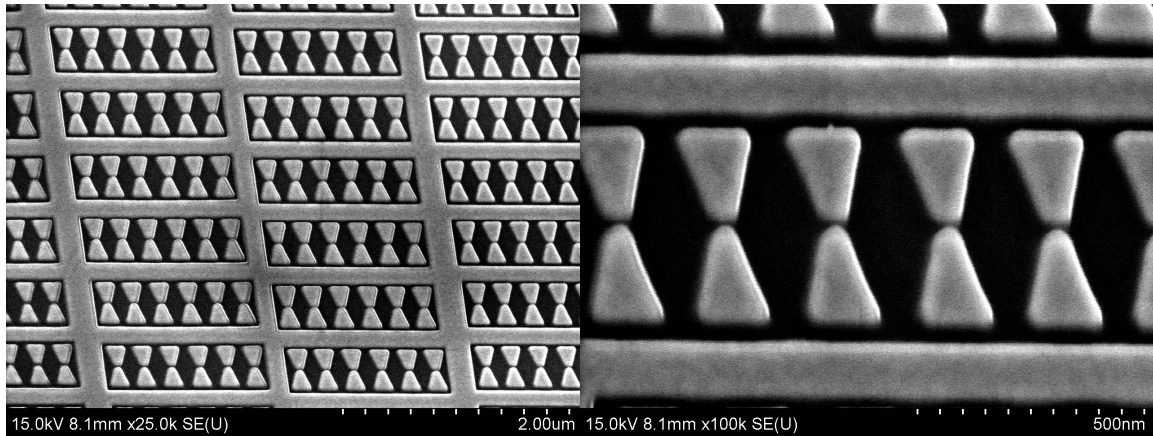


Fig. 6 SEM images of the fabricated bowtie nanostructures. Due to high magnification in imaging, edge lines are seen blurred by multiple scattering of electrons.

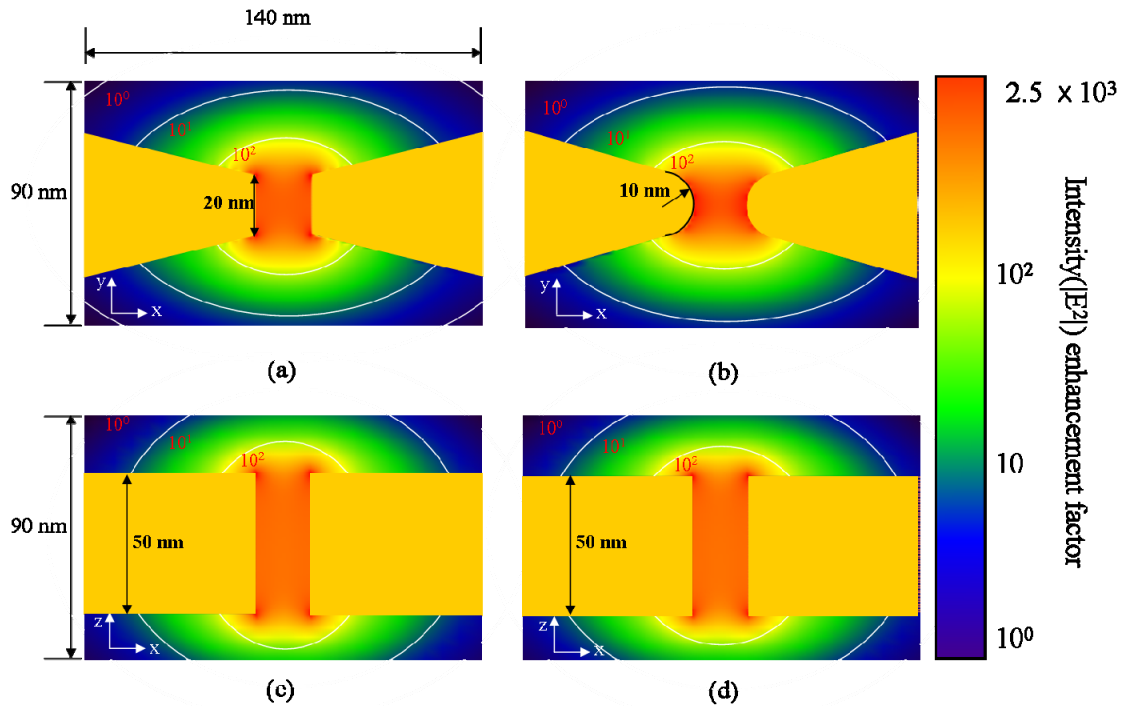


Fig. 7 Calculated near-field distributions for rounded and flat bowties; (a) top-view of trapezium bowtie (flat apex), (b) top-view of blunt bowtie, (c) side-view of trapezium bowtie, and (d) side-view of blunt bowtie. Values of the curvature of radius and the flat length are determined from the SEM images of fabricated bowtie nanostructures. This simulation reveals that the 20 dB volume is not much affected by the sharpness of the apex angle for both cases.

Another important parameter is a dwell time which decides the scanning number of FIB during fabrication. By increasing dwell time, we can minimize the broadening of the structure due to the FIB beam drift during the milling process. By repetitive adjustment of mask and condition of ion beam, 2D array of bowtie nanostructure which has the height of 175 nm, gap of 20 nm, and angle of 30 ° was fabricated. These bowties can cover the 5 μm spot size of focused femtosecond pulse laser. Each bowtie is separated by 200 nm in horizontal and 550 nm in vertical. In SEM image, shapes of apexes and edges look blur due to the multiple scattering of electrons and non-conducting sapphire substrate in imaging. It is estimated that each apex has effective radius of curvature around 10 nm. From this assumption, we conduct the calculation of near-field distribution. The results shows that the volume of enhanced near-field over 20 dB didn't quite decrease as expect, so high harmonic generation can be induced with this kinds of nanostructure.

4. EXPERIMENTS

To generation of high harmonics, fabricated bowtie nanodevice was placed in the vacuum chamber shown in fig. 8. All experiment was conducted in vacuum condition to prevent absorption of EUV by ambient air. Femtosecond laser was focused from clean the sapphire substrate to gold bowties with precise control of group delay dispersion. The focused laser beam has a size of 5 μm in diameter (FWHM) and peak intensity of $3.6 \times 10^{11} \text{ Wcm}^{-2}$ which is 2 order of magnitude lower than necessary intensity for high harmonic generation. The group delay dispersion by chamber window, focusing lens, sapphire substrate was compensated by the pair of chirped mirror and wedge. Using optical correlation technique, pulse duration of femtosecond pulse laser after passing trough dispersion medium and compensating was measured as 11 ~ 12 fs. In this experiment, a gas jet of argon & xenon were injected continuously through a metal nozzle which has inner diameter of 100 μm. The back pressure of gas jet was set as 115 torr controlled by the mass flow controller.

Fig. 9 shows spectrum of generated high harmonics. When Xenon gas was injected, odd harmonics up to 21st order can be detected by spectrometer which was consisted by varied line spacing grating (Hitachi, 001-0639) and photon multiplier (Photonics, 4751G CSI). H3 (266 nm), H5 (160 nm) was not seen in spectrum because they are out of range of wavelength detector. The photon multiplier is located at a distance of 469 mm from the varied line spacing grating that disperse the light in the wavelength range of 22 nm - 124 nm. The photon multiplier is mounted on a precision stage moving along the dispersing line of the grating. The photon multiplier used here is sensitive to high harmonic radiation only below 200 nm in wavelength, hence no metallic filter was used for block fundamental femtosecond laser. The grating has a narrow acceptance angle of $\pm 1.0^\circ$, which provides a 1.0 nm resolution of wavelength division for each 1.0 mm spatial position. For resolving precisely, a slit of a width of 1.0 mm was attached to a photon multiplier to avoid the effect of excessive convolution in the measured data. Given that the input femtosecond laser provides a small peak power of 100 kW, the observed harmonics yield relatively low power in the range of a few nW in total. However, the conversion efficiency with argon gas was found to be in the level of 2.4×10^{-9} for H7 and all the way down to 6.9×10^{-10} for H17, which is comparable to those of CPA. However, harmonic generation with xenon gas shows more efficient energy conversion of 10^{-8} which is generally observed in generation of high harmonics.

The spatial distribution of emitted high harmonics treated as the interference pattern by the 2D array of dipolar radiation source. The intense spot of focused femtosecond pulse on the surface of the nanostructure has a 5 μm diameter, which involves approximately 150 bowties simultaneously in high harmonic generation. Each bowtie could be approximate as a dipolar source that radiates high harmonics with a broad angle distribution. These multiple interferences cause the particular spatial diffraction pattern that the nanostructure would produce as a 2-dimensional diffractive grating as a whole. For instance, H17 harmonic of 47 nm wavelength has the first-order diffraction angle of 13.6° in one direction and 4.9° in the other direction, with other higher-order diffraction angles being larger than those of the first-order angles. In the experiment, only the 0th-order diffraction of H17 harmonic was collected by the photon multiplier, because all other diffraction angles lie beyond than the acceptance angle of $\pm 1.0^\circ$ of the spectrometer used, and this is also the case for other detected harmonics of H7 - H15. Obviously all the 0th-order diffracted rays of the generated harmonics proceed in the same propagation direction of the incident femtosecond pulse, thereby residing within a narrow cone-shaped $\pm 7^\circ$ angle distribution being formed in response to the focusing angle of the incident pulse. An additional concern was the dispersion-induced phase mismatching due to the interaction of generated harmonics with the injected argon gas. However, no particular attention was paid to this problem since the field enhancement for high

harmonics generation is confined to a short length of less than 1 micrometer as the incident femtosecond pulse passes through bowties.

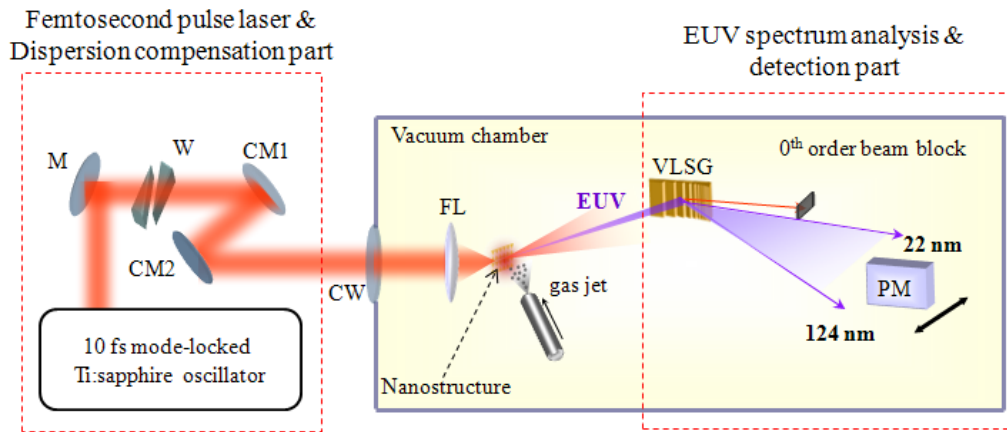


Fig. 8. Experimental apparatus for high harmonic generation with plasmonic nanostructures. The whole system is conveniently divided into three parts; i) Dispersion controlled femtosecond pulse laser source on the left, ii) Fabricated nanostructure and injecting module of gas jet in the center, and iii) EUV spectrum analysis by a dispersive grating and photon multiplier. CM, chirped mirror; CW, chamber window; FL, focusing lens; M, mirror; PM, photon multiplier; VLSG, varied-line-spacing grating; W, wedge plate;

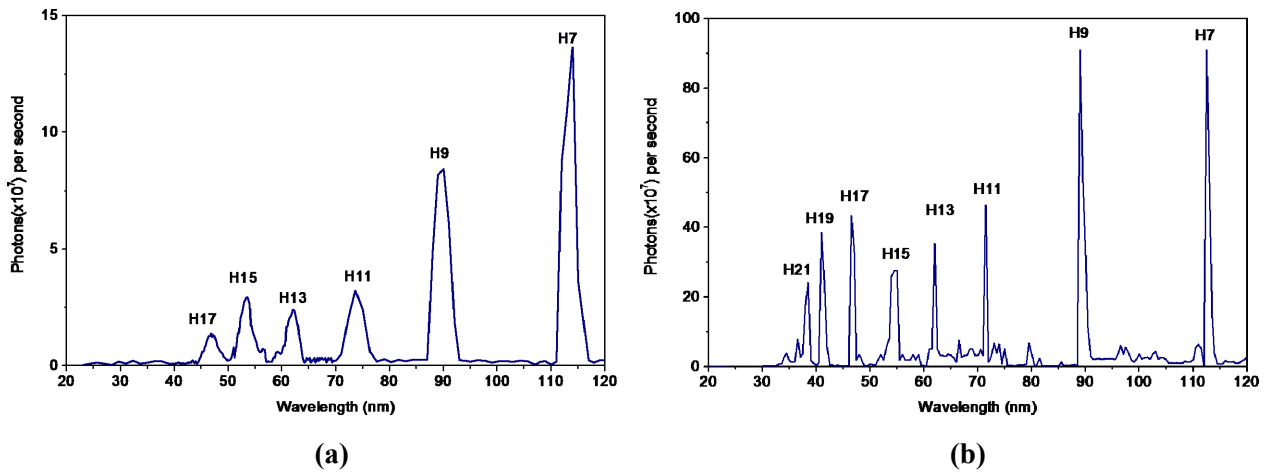


Fig. 9 High harmonics generated by plasmonic enhancement with injection of argon (a) and xenon gases (b). A varied-line-spacing grating was used to disperse the 22-124 nm wavelength band. H7, H9 and H21 were collected by moving a photon multiplier in fine steps along the disperse line. The aperture of the photon multiplier was covered by a slit of 1.0 mm width to reduce the convolution of neighbouring harmonic signals. Given the input pulse power of 100 mW, the efficiencies for the harmonics were different with gas in use. The xenon injection shows more efficient photon emission than that of argon injection.

From the cut-off frequency of high harmonics, we can expect the enhanced femtosecond laser intensity around bowtie nanostructure. As shown in following equation,

$$E_{\text{cut-off}} = I_p + 3.17U_p \tag{1}$$

Where E_{\max} is maximum energy of harmonic photons, I_p is ionization energy of xenon, U_p is ponderomotive potential. For a linearly polarized oscillating field, U_p has a form of

$$U_p = 9.33 \times 10^{-14} I_L \lambda^2 \quad (2)$$

Where I_L is the intensity, λ is the wavelength of incident femtosecond laser. From the generated harmonic spectrum of xenon injection, E_{\max} can be set as 32.6 eV, because maximum harmonic is 21st order. By adopting 1st ionization energy of xenon (12.1 eV), enhanced laser intensity of femtosecond laser was calculated as $1.1 \times 10^{14} \text{ Wcm}^{-2}$. For the case of argon injection, laser intensity of as $5.4 \times 10^{13} \text{ Wcm}^{-2}$ which is 2 times smaller than that of xenon injection even same intensity of input laser. The intensity enhancement by the bowtie nanostructure can be expected as more than 100 times. As considered in FDTD calculation, intensity enhancement factor of 1000 could be formed within a gap of bowtie nanostructure, but effects by such a high intensity enhancement was not detected. Because the area of higher intensity enhancement is as small as few cubic nm, optical power of emitted high harmonic is too low to detect the signal. Generally, high harmonic generation with argon can obtain higher order than that of xenon, because argon has higher ionization energy than xenon. When we assume that actual local field enhancement occur as same as xenon, maximum order of high harmonic must be observed at 23rd order (34 nm in wavelength) with injection of argon gas. However, high harmonics shown in spectrum had maximum order of 17th (47 nm in wavelength) which is 3 steps lower than the experiment. One reason of cut-off at 17th seems to be conversion efficiency of high harmonic generation with argon gas. Because energy conversion efficiency of argon is lower than xenon, emitting optical power of generated harmonics higher than 17th seems to be too low to detect photon multiplier. Energy conversion efficiency of overall harmonics is around 10^{-8} which is lower than traditional way of high harmonic generation using CPA. This is due to the short interaction length along the femtosecond laser propagation direction and diffracted emission property. In case of high harmonic generation using CPA, a femtosecond pulse laser was focused loosely to lengthen the depth of focus, which represents the longest interaction volume along the optical axis. Enhanced intensity distribution by FDTD calculation showed existence of high intensity enhancement factor over 30 dB, but it didn't make a significant influence in generation of high harmonics.

For acquiring higher localize surface plasmons, excitation of longer wavelength can be useful because negative real part of dielectric constant has higher absolute value for a longer wavelength. To extend the spectrum of high harmonics to a shorter wavelength, increment of input excitation laser is limited by the heat accumulation in bowtie nanostructure. Therefore, local field enhancement with proper excitation wavelength selection could give the extension of high harmonic spectrum.

5. CONCLUSION

The bowtie nanostructure tested in this study is able to enhance the pulse intensity of the incident femtosecond laser by surface plasmon resonance to generate high harmonics up to 21st order. The FDTD calculation performed here for the simulation of localized surface plasmon resonance around the bowtie nanostructure well matches with experimental results obtained by fabricating the designed bowties using the focused ion beam process. This new way of high harmonic generation enables conservation of the MHz repetition rate due to the strong enhancement effect of the localized surface plasmon, demonstrating the possibility of serving as a novel tool for fundamental studies in high order nonlinear optics. Finally, this approach could generate EUV without conventional chirped pulse amplification, so that it can form the basis for constructing laptop-sized EUV light sources to be exploited for advanced spectroscopy and microscopic applications.

ACKNOWLEDGEMENTS

This work was supported by the Creative Research Initiative Program of the Ministry of Science and Technology of the Republic of Korea.

REFERENCES

- [1] Corkum, P. B., "Plasma perspective on strong-field multiphoton ionization," *Phys. Rev. Lett.* 71, 1994-1997 (1993).
- [2] Lewenstein, M., Balcou, P., Ivanov, M. Y., L'Huillier, A. and Corkum, P. B., "Theory of high-harmonic generation by low-frequency laser fields," *Phys. Rev. A* 49, 2117-2132 (1994).
- [3] Chang, Z., Rundquist, A., Wang, H., Murnane, M.M. and Kapteyn, H.C., "Generation of coherent soft X rays at 2.7 nm using high harmonics," *Phys. Rev. Lett.* 79, 2967-2970 (1997).
- [4] Strickland, D., Mourou, G., "Compression of amplified chirped optical pulses," *Opt. Comm.* 56, 219-221 (1985).
- [5] Seres, J., Seres, E., Verhoef, A.J., Tempea, G., Strelci, C., Wobrauschek, P., Yakovlev, V., Scrinzi, A., Spielmann, C., Krausz, F., "Laser technology: Source of coherent kiloelectronvolt X-rays," *Nature* 433, 596 (2005).
- [6] Gohle, C., Udem, T., Herrmann, M., Rauschenberger, J., Holzwarth, R., Schuessler, H. A., Krausz, F., Hänsch, T. W., "A frequency comb in the extreme ultraviolet," *Nature* 436, 234-237 (2005).
- [7] Jones, R.J., Moll, K.D., Thorpe, M.J., Ye, J., "Phase-coherent frequency combs in the vacuum ultraviolet via high-harmonic generation inside a femtosecond enhancement cavity," *Phys. Rev. Lett.* 94, 193201 (2005).
- [8] Kim, S., Jin, J., Kim, Y.J., Park, I.Y., Kim, Y., Kim, S.W., "High-harmonic generation by resonant plasmon field enhancement," *Nature* 453, 757-760 (2008).
- [9] Nisoli, M., "Nanoplasmonics: Brave new attoworld," *Nature Photonics* 1, 499-500 (2007).
- [10] Roth, R.M., Panoiu, N.C., Adams, M.M., Osgood, R.M., Neacsu, C.C., Raschke, M.B., "Resonant-plasmon field enhancement from asymmetrically illuminated conical metallic-probe tips," *Opt. Express* 14, 2921-2931 (2006).
- [11] Schatz, G.C., Van Duyne, R. P., [Handbook of Vibrational Spectroscopy Vol. 1], John Wiley & Sons Ltd, Chichester, 759-774, (2002).
- [12] Sun, W.X., Shen, Z.X., "Optimizing the near field around silver tips," *J. Opt. Soc. Am. A* 20, 2254-2259 (2003).
- [13] Stockman, M.I., "Nanofocusing of optical energy in tapered plasmonic waveguides," *Phys. Rev. Lett.* 93, 137404 (2004).
- [14] Mühlischlegel, P., Eisler, H.J., Martin, O.J.F., Hecht, B., Pohl, D.W., "Resonant optical antennas," *Science* 308, 1607-1609 (2005).
- [15] Jin, E. X., Xu, X., "Enhanced optical near field from a bowtie aperture," *Appl. Phys. Lett.* 88, 153110 (2006).
- [16] Gai, H., Wang, J., Tian, Q., "Modified Debye model parameters of metals applicable for broadband calculations," *Appl. Opt.* 46, 2229-2233 (2007).
- [17] Fromm, D.P., Sundaramurthy, A., Schuck, P.J., Kino, G. and Moerner, W. E., "Gap-dependent optical coupling of single "bowtie" nanoantennas resonant in the visible," *Nano Lett.* 4, 957-961 (2004).